

Large eddy simulation of compartment fire flow with respect the effects of geometrical characteristics of compartment on its performance

¹R.Khaksari Haddad *, ²G. Heidarinejad, ³H. Pasdarsahri

¹Master of Energy Conversion, Science and Research, Islamic Azad University, Arak, Iran

²Department of Mechanical Engineering, Tarbiat Modares University, Tehran, Iran

³ Ph.D. in Mechanical Engineering, Tarbiat Modares University, Tehran, Iran

*razielh_khaksari@yahoo.com

Abstract: An important part of fire safety plan in a compartment is prediction of fluid flow. Simple empirical equations, zone models or field models are usable tools which fire safety engineers refer to them to simulate fire in an enclosure. In this study, the simulation is investigated by means of Large Eddy Simulation model which incorporates Smagorinsky turbulence model to simulate large-scale pool fire in a compartment with dimension of 3.6*3*2.4 m and an opening in the roof and one opening door in front wall is presented. Fire Dynamics Simulator (FDS), which is a Computational Fluid Dynamics (CFD) model, is used to investigate fire flow and smoke flow. Two different values of heat release rate (330 and 440kW) and ventilation roof openings (0.75*1m and 0.5*1m) are covered. For different configurations, the effect of heat release rate examined on the temperature variations and velocity variations in vertical direction in the compartment. The results show the temperature rises as HRR increases strongly. Finally, the profiles of mean temperature with respect to ambient conditions have reasonable agreement with the experimental values.

[R.Khaksari Haddad, G. Heidarinejad, H. Pasdarsahri. **Large eddy simulation of compartment fire flow with respect the effects of geometrical characteristics of compartment on its performance.** *World Rural Observ* 2018;10(4):69-76]. ISSN: 1944-6543 (Print); ISSN: 1944-6551 (Online). <http://www.sciencepub.net/rural>. 10. doi:[10.7537/marswro100418.10](https://doi.org/10.7537/marswro100418.10).

Keywords: eddy simulation, compartment fire flow, geometrical characteristics of compartment

Introduction

Accurately prediction of the consequences of fires to evaluate the fire safety and appropriate design of fire protection devices is very important. Among the various methods to predict the consequences of fires, use of numerical methods for predicting the spread of smoke and transient temperature distribution and also velocity is emphasized. though still the current understanding of the mechanisms of various phenomena such as convection, buoyancy and buoyancy fluid motion, turbulence, chemical combustion, soot formation and radiative heat transfer has not yet fully achieved [1] but much research have been done in this field. The ultimate goal of numerical simulations is predicting the behavior of complex, transient fire that lead to simulation of different scenarios to enhance the human safety.

With the rapid development of computer, an efficient tool for fire safety risk assessment is provided [2] that using of computational fluid dynamics (CFD) and in particular large eddy simulation (LES) codes to model fires. Compared with laboratory measurements and hand calculations, computational fluid dynamics (CFD) offers a more comprehensive analysis. However, in order to increase the reliability of the CFD calculations in real room fires, it is necessary to compare numerical calculations with experimental data for different scenarios. The

software package, Fire Dynamics Simulator (FDS), a LES code with a post-processing visualization tool, SMOKEVIEW, developed by National Institute of Standards and Technology (NIST), USA is now a practical tool for simulating fire environment. In this software, Navier - Stokes equations are solved with assuming a low Mach number fluid flow and with an emphasis on smoke and heat transport. This model has been subjected to numerous validation and calibration studies on temperature and velocity field distribution in normal sized room fires [3–5]. It was also applied to study the dispersion of propane under a leakage condition in a room [6] and contamination levels in near and far field in a warehouse facility under forced ventilation [7]. However, how good the gas concentration distribution in the fire-induced smoke flow will be predicted by FDS has rarely been addressed.

In this study, we focused on simulation of compartment pool fire with natural ventilation. In compartment fire simulation, mass flow rate, temperature and neutral plate height that are parameters used to simulate the flow in the opening. Understanding the air flow rate and neutral plate position in openings is important for fire safety engineering that the ventilation factor plays an important role in predicting these parameters. These parameters have been studied by several researchers

[8-16], but few of them have examined the effect of opening area on these parameters. In this study openings are simulated on the roof and the front wall and the main objective of this study is providing insight into the flow field using computational fluid dynamics simulation. Therefore, numerical simulation results are presented for all cases have been studied in [17]. The simulation involves much more accurate information of the mean temperature and average velocity at the door opening and the effect of opening area on position of the neutral plate. Special features of this simulation are:

- The size of the fire source is large in comparison with door opening area, roof opening and compartment dimension.
- Heat release rate per unit area is relatively high.
- There is asymmetry in the roof openings' positions.

The first aim of this study is to investigate the influence of different parameters on the mean velocity and mean temperature. The parameters studied are:

- Dimensions of roof opening
- Heat release rate

Keep in mind that the heat release rate in the simulation is high (330 & 440 Kw/m²) and the flames are long compared to the height of the room, which shows good agreement between the numerical results and the experimental data.

Description of the configurations

Fig. 1 shows the compartment geometry as a 'Smokeview' picture. A complete description is provided in [17]. The dimensions are 3.6*3.0*2.4m with a door opening (0.9*2.0m) in the middle of the front wall. The one opening in the roof is of size 0.75*1m (Fig. 1). They are centrally positioned around $x = 1.8$ m. The distance between the roof opening centers and the front wall is 1 m. The fire source is positioned in the center of the compartment

at 0.3m height. The fire source area is considered: $A_f = 0.3*0.3$. Two fire heat release rate values are applied: = 330 and 440 kW. Two values of the roof opening area are used: = (0.75*1.0 m) = 0.75 and = 0.5*1.0m = 0.5.

Computational fluid dynamics simulations

In the field model simulations, performed with the NIST code FDS, thermocouples are defined in the simulations at the same positions as in the experiments of [17], and hence comparisons can be made for the mean temperature values and fluctuations. The 'THERMOCOUPLE' command is applied to report the temperatures, in order to follow the experimental procedure as closely as possible. There are thus four thermocouple trees, with coordinates $x = 0.5$ m, $y = 2.55$ m; $x = 1.8$ m, $y = 2.55$

m; $x = 3.1$ m, $y = 2.55$ m; $x = 1.8$ m, $y = 0.5$ m. Each tree contains 10 thermocouples, at the following heights: 0.2, 0.7, 1.0, 1.15, 1.3, 1.45, 1.6, 1.75, 1.9 and 2.05 m.

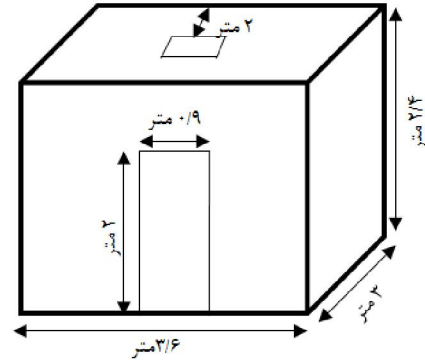


Figure 1. compartment layout

Furthermore, vertical planes are defined through the center of the side walls ($y = 1.5$ m) and the center of front (and back) wall ($x = 1.8$ m), as well as horizontal planes at $z = 1.0$, 1.5 and 2.0 m. As such, contour plots are presented of temperature and velocity providing insight into the Phenomena. External wind is neglected. In the experiments, care was taken that the influence of wind is small [17]. The fire is prescribed as a steady heat release rate per unit area, supplying the fuel with the correct mass flow rate in a horizontal plane at height 0.3m and area

equal to A_f . In the experiments, a small amount of additional air was supplied in order to enhance turbulent mixing and combustion [17]. This additional airflow is neglected in the simulations. Turbulence is modeled by the large-Eddy simulations (LES) technique in FDS. The standard Smagorinsky model is used, with constant $C_s = 0.20$. The situation is a relatively large fire source in a relatively small compartment.

As a result, LES can indeed be accurate, because a sufficient amount of grid cells can be used [4]. Here, we apply cubic cells with size 5 cm. The resulting mesh is 60*50*40 = 120,000 cells. This corresponds to at least 10 cells in each direction in the plume above the fire source, which is generally considered sufficient [18]. In general, the default FDS settings have been applied. For details the reader is referred to the technical reference guide [5]. Only a few aspects are highlighted here. Ambient temperature is set equal to ambient conditions in the experiments ([17]). Radiation is taken into account by means of a finite volume method. The combustion model is the mixture fraction-based flame sheet model, and hence the flame is in principle a surface at stoichiometric mixture

fraction. The default thermal wall boundary condition, applied in the present study, is a combination of convection and conductive heat loss through the walls and the ceiling. Their thickness is 15 cm and their thermal properties are: $\rho = 900$, $c = 900$ and $k = 0.2$. The implementation details in FDS are well documented in [5] and are not repeated here. The default velocity boundary conditions, as implemented in FDS [5], have been applied.

Theoretical analysis

A pool fire is a diffusion flame driven entirely by gravitational buoyancy. Nevertheless, it possesses many of the characteristics of non-buoyant jet diffusion flames [19, 20]. It is convenient to divide the pool fire into two parts; the combustion zone and the upper plume zone. In the combustion zone, fuel and air are mixed and react to form products in stoichiometric proportions. The burned gas axial velocity increases rapidly in the vertical direction, as do the vertical fluxes of mass, momentum and thermal energy in the fire. In the plume zone, which begins at the upper edge of the combustion zone where all the fuel has been consumed, there is no further increase in thermal energy flux, yet the mass and momentum fluxes continue to increase. Continued air entrainment is accompanied by declines in temperature, concentration of combustion products, and axial speed. In the following subsections, we develop integral forms for the conservation of mass, energy, and momentum for the flow in the pool fire.

The fluid motion of the fire is assumed as low speed flow. The contribution of acoustic waves is considered to be negligible to the flow dynamics [21, 22]. The low Mach number Favre-filtered mass, momentum, energy and scalar conservation equations in Cartesian coordinate can be written as:

$$\frac{\partial \bar{\rho}}{\partial t} + \frac{\partial (\bar{\rho} \tilde{u}_i)}{\partial x_i} = 0 \quad (1)$$

$$\frac{\partial (\bar{\rho} \tilde{u}_j)}{\partial t} + \frac{\partial (\bar{\rho} \tilde{u}_i \tilde{u}_j)}{\partial x_j} = -\frac{\partial \bar{p}}{\partial x_i} + \frac{\partial \bar{\tau}_{ij}}{\partial x_j} + \frac{\partial \bar{\tau}_{u_i u_j}}{\partial x_j} + \bar{\rho} g_i \quad (2)$$

$$\bar{\rho} C_p \frac{\partial \bar{T}}{\partial t} + \bar{\rho} C_p \tilde{u}_i \frac{\partial \bar{T}}{\partial x_i} = \frac{D \bar{p}}{Dt} - \frac{\partial \bar{q}_i}{\partial x_i} + \frac{\partial \bar{\tau}_{u_i T}}{\partial x_i} + \bar{\omega}_T + S_{rad} \quad (3)$$

$$\frac{\partial (\bar{\rho} \tilde{\phi})}{\partial t} + \frac{\partial (\bar{\rho} \tilde{u}_i \tilde{\phi})}{\partial x_i} = -\frac{\partial \bar{q}_\phi}{\partial x_i} + \frac{\partial \bar{\tau}_{u_i \phi}}{\partial x_i} + S_\phi \quad (4)$$

Where ρ is the mixture density, u_i is the velocity vector, p is the pressure, and T is the temperature. From above, ϕ represents the scalar quantities involve in the flow system while ω_T represents the filtered heat release source term. S_{rad} and S_ϕ , describe the global radiative heat exchange and generation rate of species, respectively.

The filtered viscous stress tensor, heat flux vector and species diffusion vector can be calculated using Newton's, Fourier's and Fick's law respectively by:

$$\tau_{ij} = -\frac{2}{3} \mu \frac{\partial \tilde{u}_k}{\partial x_k} + \mu \left(\frac{\partial \tilde{u}_i}{\partial x_j} + \frac{\partial \tilde{u}_j}{\partial x_i} \right) \quad (5)$$

$$\bar{q}_i = -\frac{\mu C_p}{Pr} \frac{\partial \bar{T}}{\partial x_i} \quad (6)$$

$$\bar{q}_\phi = -\frac{\mu}{Sc_\phi} \frac{\partial \tilde{\phi}}{\partial x_i} \quad (7)$$

The molecular Prandtl and Schmidt number are set to 0.7 [21]. The unknown SGS correlation

appearing in Eq. (2) ($\bar{\tau}_{u_i u_j}$) requires closure using SGS models. In the current study, two different approaches will be used and compared for the closure model. Previously, Smagorinsky-Lilly model [23] successfully applied for the simulation of jet and buoyant fire [21, 24]. In this SGS model, the Smagorinsky-Lilly SGS correlation can be modeled using following expressions:

$$\bar{\tau}_{u_i u_j} = \bar{\rho} \widetilde{u_i u_j} - \bar{\rho} \tilde{u}_i \tilde{u}_j = -2 \mu_t^{SGS} \tilde{S}_{ij} + \frac{1}{3} \bar{\tau}_{kk} \delta_{ij} \quad (8)$$

$$\tilde{S}_{ij} = \frac{1}{2} \left(\frac{\partial \tilde{u}_i}{\partial x_j} + \frac{\partial \tilde{u}_j}{\partial x_i} \right) - \frac{1}{3} \frac{\partial \tilde{u}_k}{\partial x_k} \delta_{ij} \quad (9)$$

$$\mu_t^{SGS} = \bar{\rho} C_s \Delta^2 |\tilde{S}_{ij}| \quad (10)$$

Previous studies suggested that $\bar{\tau}_{kk}$ may be ignored [25]. In Eq. (10), Δ is the sub-grid length and is defined as $\Delta = (\Delta x \Delta y \Delta z)^{1/3}$, μ_t^{SGS} is the Smagorinsky SGS turbulence viscosity and C_s is the Smagorinsky constant and taken into 0.2 [21].

Results

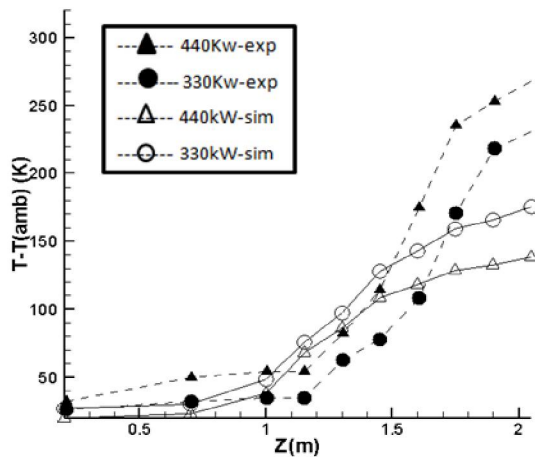
Fig.2 shows mean temperature profiles with respect to ambient conditions ($T_f - T_{amb}$). As in [17], averages are taken by three thermocouple trees behind the burner. All profile shapes are similar, with a plateau of relatively low temperature below the height $Z = 1.2m$ (cold lower layer). Clearly, the same trends are observed in the simulation results (lines) when compared with the experiment results (symbols). In both columns, a decrease in the mean temperatures is observed as the roof opening area increases.

The general trends are very well reproduced in the numerical simulations. The numerical trends are very similar to the experimental profiles for all configurations. Still, the temperatures are lower in the

numerical simulations than in the experiments. The first reason is higher heat loss through the walls and ceiling in the numerical simulations than in the experiments. Another possible reason is over-estimation of entrainment of fresh air into the smoke in the numerical simulations, which causes lower average temperatures in the simulations. Despite the possible errors mentioned, as we consider agreement between simulation results and experimental data, the CFD simulation results can be used to study flow phenomena taking place in reality. In all configurations the highest fluctuation is found around $Z=1.5$ m, corresponding to the transition zone between the cold bottom layer and the hot upper layer, which is the region with the steepest gradients in the mean temperature profiles (Fig. 2).

$$A_f = 0.3\text{m} \times 0.3\text{m}$$

$$A_{\text{roof}} = 0.5\text{m} \times 1.0\text{m}$$



$$A_f = 0.3\text{m} \times 0.3\text{m}$$

$$A_{\text{roof}} = 0.75\text{m} \times 1.0\text{m}$$

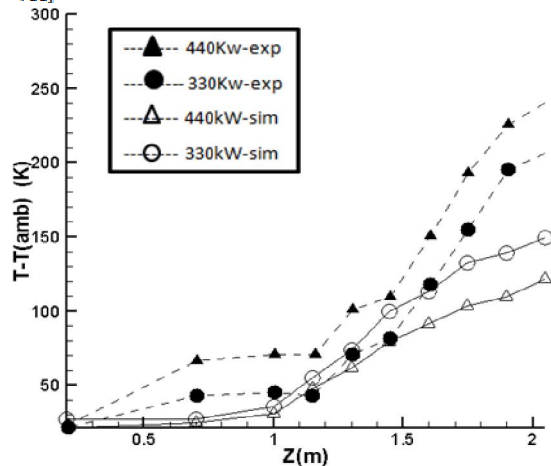


Fig. 2. Mean temperature profiles (averages taken over the three thermocouple trees behind the burner) (solid lines: simulation results; dashed lines: experiments).

Figure 3 indicates a complete schema of the mean temperature and fluid flow in the horizontal center plane. The mean temperature contours are plotted over the last minute of simulations (i.e. from 60 to 100s). The global movement in the plane $Y = 1.5$ is upward, with the downward motion in the corners, the flow is almost symmetric. This result is entirely consistent with the temperature contour. Note that flow is leaving the compartment through the roof opening and the upper part of the vertical door opening. Near the ceiling, impingement is visible; in the upper right corner, smoke flows toward the rear wall ($y = 3\text{m}$) ($V > 0$), while the opposite is seen in the upper left corner. Note that the impingement point is located at $Y = 1.5$ m above the fire source. At the bottom of the plume, cold fresh air is entered from both sides and rotating hot flows in the upper corners do not move toward the floor, so cold air is entered from back side of the plume, not cold smoke. As mentioned, rotating regions are observed at both sides of the plume, with downward smoke motion. Note that the plume remains circular and clearly visible, with strong moves from the floor to the ceiling. Also the smoke flows out of the room through the door opening. At a height of 1.5 m, the plume shape is less circular, as can be seen in the temperature contours.

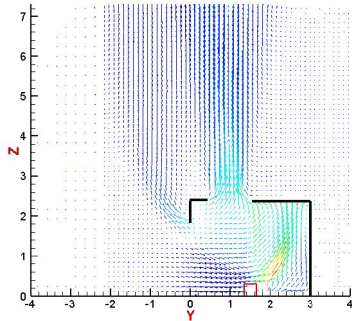
Impingement point is closer to the back wall to the front wall. This phenomenon influences the average temperature; High temperature region is thicker at the right side than at the left side. This phenomenon is also due to hot smoke enters the compartment through the door at a height of between 0 m and 1.6 m and it causes the plume is tilted toward the back wall. As expected in a fire, the temperature near the flame is higher than the temperature near the roof. When the fire plume moves upward and incoming plume joins, the temperature decreases from the center to the top. Clearly, the highest temperatures are found above the fire source. The main result obtained is that the temperature near the door opening is lower than the rear wall because the fresh air entrains into the room and the flame is tilted backward.

Near the flame, the V component is positive which exhibits the arrival of fresh air into the plume (see also Fig. 3). The flame is tilted toward the rear wall in the Y -direction due to the entrainment of air through the door; negative V values at the left side and the positive velocity values at the right side. Note that the flame tends to be drawn to the left wall, because the roof opening is on that side. Highly negative V values are displayed near the ceiling. This is due to the combined effect of impingement of the plume toward the ceiling at a region with height of 1.8 m versus $y = 1.5$ m and upward moves of smoke to the roof opening, which is located closer to the front wall.

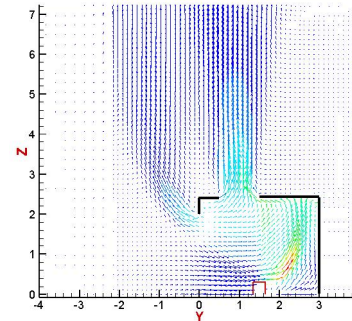
The velocity contour represents a sharp upward motion in the plume, which is due to buoyancy. V and W velocities combination indicates that fresh air enters into the compartment, flows to the plume and wraps around it, so the plume to be tilted towards the back wall. The most noticeable motion is upward; the region with high W velocities is related to the high temperature region. At Z=1.5 m, impingement and

plume stretching is still remains and V values are considerably smaller than plane Z = 1.0 m. So stretching and compression is less intense. Flame moves toward the back wall at a height of 2 m evidently. Especially, in the upper left corner, there is a region of larger negative velocity values that shows the smoke moves towards the roof opening.

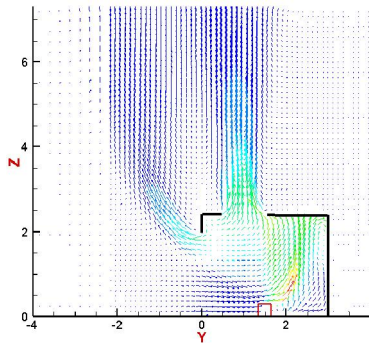
HRR=440kw
Roof vent=0.75m*1m



HRR=330kw
Roof vent=0.75m*1m



HRR=330kw
Roof vent=0.5m*1m



HRR=440kw
Roof vent=0.5m*1m

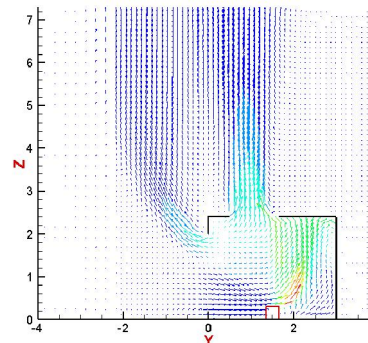
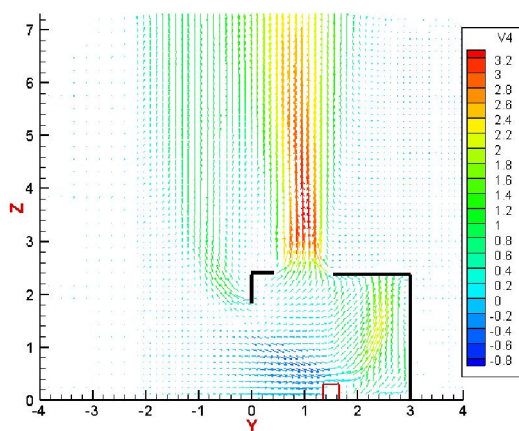


Fig. 3. Mean velocity components and temperature (°C) in horizontal plane y = 1.5 m.

HRR=330kw
Roof vent=0.75m*1m



HRR=440kw
Roof vent=0.75m*1m

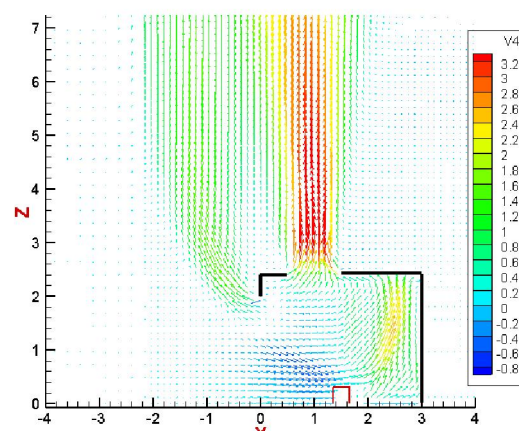
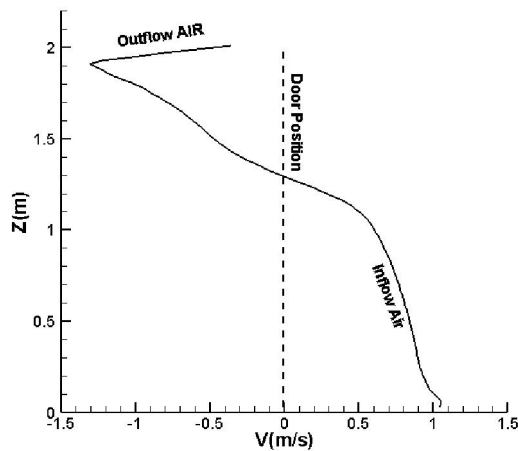


Fig. 4. Influence of heat release rate on velocity in horizontal plane y=1.5m

As heat release rate increases, the liquid fuel is evaporated more rapidly and higher temperatures are more likely to produce pyrolysis and enhanced soot formation near the fuel source. Large amount of heat leaves the compartment through the roof opening and door opening. Figure 4 shows that the mean temperature near the back wall is decreased in numerical simulation due to the heat release rate reduce. Also, the rate of exhaust flow, which leaves the compartment through the door opening, is influences hardly by heat release rate. One of the most

important macroscopic parameter is the mass flow rate of air which enters to fire room. This parameter may be affected by the heat release rate and also opening area. The inflow mass flow rate is calculated by integrating the normal velocity at the opening. The results show that with an increase in HRR, the inflow mass flow rate significantly increases. In the situation with same HRR, reducing in the area of opening causes a significant decrease in the mass flow rate of the air inflow.

HRR=440kw
Roof vent=0.5m*1m



HRR=440kw
Roof vent=0.75m*1m

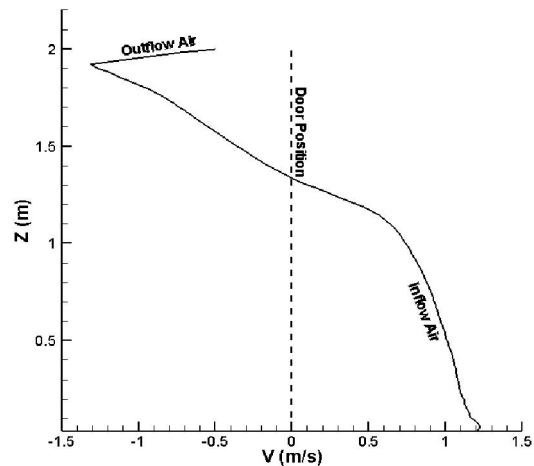
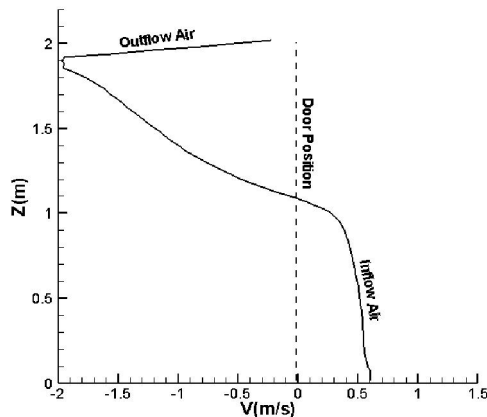


Fig. 5. Mean velocity components at door opening position

Fig.5 shows that there is smoke flow through the upper part of the vertical door opening. Actually hot smoke leaves the compartment through the door between $Z=1.4$ and 2.0m and cold air enters the compartment through the door between $Z=0$ and

1.4m ; negative V component values at the left side and positive values at the right side. Note that the velocity of cold air is increased when the roof opening area increases (approximately 1m/s in comparison with about 1.2m/s).

HRR=440kw
Without Roof vent



HRR=440kw
Roof vent=0.75m*1m

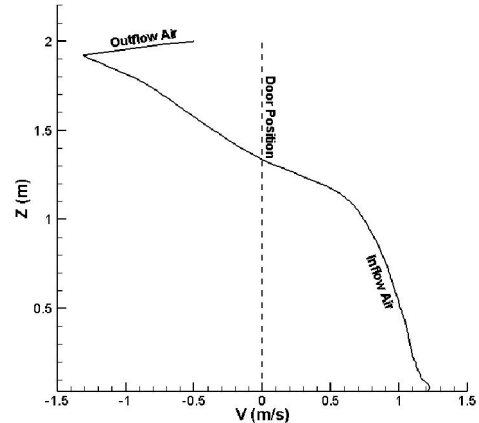


Fig. 6. Mean velocity components at door opening position (with roof opening and without roof opening)

Fig.6. shows the differences between velocity parameters at door opening when compartment has roof opening and when it does not. This figure indicates that the maximum measured outflow velocity increases (from about -1.3m/s to approximately -2m/s) in upper edge of the door opening as the roof opening is deleted, however, accompanied by a substantial decrease in cross-flow velocity of cold air in lower edge of the door opening (at approximately $z=0.0$) in the numerical simulations. In other words, inflow air velocity decreases when the roof opening is deleted.

Conclusion

This current work particularly examines a single room compartment fire dynamics with a door opening and a ventilation opening in the roof. The main achievement of this study here is to investigate how heat release rate and roof opening area effect on the environment of the enclosure. CFD simulation results are obtained by FDS. Therefore, the behavior of the structure of the compartment fire is recognized by means of this numerical study. Large-Eddy-Simulation coupled with Smagorinsky subgrid model to predict temperature contours and velocity contours.

The following aspects have been confirmed:

- The global motion is upward and flow leaves the compartment through the roof opening and the upper part of door opening.

- The flame is tilted toward the rear wall in the Y-direction due to the entrainment of air through the door.

- The general trend of numerical simulation of $(T_{av} - T_{amb})$ is similar to experimental results.

- The average temperature rise $(T_{av} - T_{amb})$ increases clearly as the fire heat release rate rises. Due to the smoke mass flow rate is become different through the opening, this phenomena happened.

- The mean temperature near the back wall decreases as HRR decreases.

- The rate of exhaust flow, which leaves the compartment through the door opening is practically unaffected by HRR.

- The inflow mass flow rate significantly increases as HRR increases.

- Temperature increases near the roof as A_{roof} increases, due to increased smoke mass flow.

- Cross-flow velocity at the roof opening increases, in particular for the biggest A_{roof} values.

- When the roof opening is deleted, V-velocity values decrease in the bottom edge of door opening

but cross-flow velocity and mean temperature is increased near the door opening.

- The mean temperature and velocity near the fuel source increase as the roof opening deleted.

References

1. D. Drysdale, in: An Introduction to Fire Dynamics, second ed. Wiley, New York, 1999.
2. W.K. Chow, Application of computational fluid dynamics in building services engineering, Build. Environ. 31 (1996) 425–436.
3. J. Sutula, Applications of the Fire Dynamics Simulator in fire protection engineering consulting, Fire Protect. Eng. (2002) 33–43.
4. P.A. Friday, F.W. Mowrer, Comparison of FDS Model Predictions with FM/SNL Fire Test Data. NISTGCR01-810, National Institute of Standards and Technology, Gaithersburg, MD, 2001.
5. K.B. McGrattan, G.P. Forney, Fire Dynamics Simulator (Version 4.07)—User’s Guide. NIST Special Publication 1019, National Institute of Standards and Technology, Gaithersburg, MD, 2006.
6. N.L. Ryder, J.A. Sutula, C.F. Schemel, A.J. Hamer, V.V. Brunt, Consequence modeling using the Fire Dynamics Simulator, J. Hazard. Mater. 115 (2004) 149–154.
7. N.L. Ryder, C.F. Schemel, S.P. Jankiewicz, Near and far field contamination modeling in a large scale enclosure: Fire Dynamics Simulator comparisons with measured observations, J. Hazard. Mater. 130 (2006) 182–186.
8. Prah, J. and Emmons, H. W., “Fire Induced Flow through an Opening,” Combustion and Flame, 25 (3), pp. 369-385, 1975.
9. Rockett, J. A., “Fire Induced Gas-Flow in an Enclosure,” Combustion Science and Technology, 12 (46), pp. 165-175, 1976.
10. Nakaya, I., Tanaka, T., Yoshida, M., and Steckler, K., “Doorway Flow Induced by A Propane Fire,” Fire Safety Journal, 10 (3), pp. 185-195, 1986.
11. Steckler, K. D., Quintiere, J. G., Rinkinen W. J., “Flow Induced by Fire in A Compartment,” NBSIR 82-2520, National Bureau of Stands, Washington, D.C., 1982.
12. Bryant, R. A., “Particle Image Velocimetry Measurements of Buoyancy Induce Flow through a Doorway,” NISTIR 7252, National Institute of Standards and Technology, Gaithersburg, MD, 2005.
13. Bryant, R. A., and Johnson E. L., “Large-Scale Particle Image Velocimetry Measurements of a Fire Induced Doorway Flow,” Proceedings of

- Combustion Institute/Eastern States Section, pp. 178-180, Orlando, FL, Nov. 2005.
14. Shaddix, C. R., Allendorf, S. W., Hubbard, G. L., and Ottesen D. K., "Diode Laser Diagnostics for Gas Species and Soot in Large Fires," SAND2001-8383, Sandia National Laboratories, Albuquerque, NW, 2001.
 15. Leblanc, D., "The Use of Field Models for Determination the Performance of Water Mist Systems: A Preliminary Analysis", International Water Mist Conference, pp 39-48, Amsterdam, Netherland, April 2002.
 16. Moinuddin, K.A.M. and Thomas, I.R., "Factors Affecting Grid-independent Results for Compartment Fire Modeling," 16th Australasian Fluid Mechanics Conference, Crown Plaza, Gold Coast, Australia, Dec. 2007.
 17. B. Merci, P. Vandevelde, *Fire Saf. J.* 42 (8) (2007) 523–535.
 18. K.B. McGrattan, H.R. Baum, R.G. Rehm, *Fire Saf. J.* 30 (1998) 161–178.
 19. J.A. Fay, *J. Aero. Sci.* 21 (1954) 681–689.
 20. S.P. Burke, T.E.W. Schumann, *Ind. Eng. Chem.* 20 (1928) 998–1004.
 21. Sherman C.P. Cheung, G.H. Yeoh, A fully-coupled simulation of vertical structures in a large-scale buoyant pool fire, *Int. J. Therm. Sci.* 48 (2009) 2187-2202.
 22. S.C.P. Cheung, G.H. Yeoh, A.L.K. Cheung, R.K.K. Yuen, Flickering behavior of turbulent buoyant fires using large-eddy simulation, *Num. Heat Transf. Part A* 52 (2007) 679-712.
 23. J. Smagorinsky, General circulation experiment with the primitive equations: part I. The basic experiment, *Mon. Weather Rev.* 91 (1963) 99-164.
 24. Y. Kang, J.X. Wen, Large eddy simulation of a small pool fire, *Comb. Sci.* 176 (2004) 2193-2223.
 25. G.H. Yeoh, K.K. Yuen, *Computational fluid dynamics in fire engineering*, Elsevier Inc., 2009.

12/25/2018